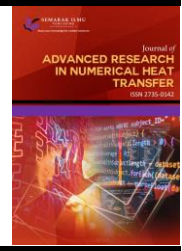




## Journal of Advanced Research in Numerical Heat Transfer

Journal homepage:  
<https://semarakilmu.com.my/journals/index.php/arnht/index>  
ISSN: 2735-0142



# Numerical Analysis of Fluid Flow and Heat Transfer Characteristics of Novel Microchannel Heat Sink

Yew Wai Loon<sup>1</sup>, Nor Azwadi Che Sidik<sup>1,\*</sup>, Yutaka Asako<sup>1</sup>

<sup>1</sup> Malaysia-Japan Institute of Technology, Universiti Teknologi Malaysia, Jalan Sultan Yahya Petra, 54100, Kuala Lumpur, Malaysia

### ARTICLE INFO

#### Article history:

Received 11 September 2023  
Received in revised form 12 October 2023  
Accepted 15 November 2023  
Available online 31 December 2023

#### Keywords:

Microchannel heat sink; secondary channels; rectangular ribs; tertiary channels; thermal resistance

### ABSTRACT

Microchannel heat sinks have gained prominence in the field of thermal management, offering compact and efficient solutions for dissipating heat flux from high performance electronic devices. Escalating heat flux in modern electronic devices, such as those found in telecommunication equipment, industrial automation equipment, solar devices, and data centre servers has driven the continuous development of microchannel heat sink to achieve efficient thermal management. The critical challenge in thermal management for these devices is to develop a microchannel that enhances heat transfer performance and minimises pressure drop. Heat transfer and pressure drop are two competing factors that determine the practicability of the design for real world application. Improvement in heat transfer performance usually results in an increase in pressure drop and pumping power. This study addresses the challenges of designing microchannel through comprehensive numerical analysis of fluid flow and heat transfer characteristics of a novel design that combines ribs, secondary channels, and tertiary channels. The numerical results showed that the novel microchannel design achieves a favourable balance between heat transfer and pressure drop, demonstrating its potential to be used in application where high heat transfer and efficiency are paramount. To assess the performance of the microchannels, thermal resistance, a measure of system's resistance to heat transfer is used. At the same pumping power, thermal resistance in the new design is consistently lower compared to other designs.

## 1. Introduction

Heat removal is a natural phenomenon that occurs in various processes on Earth such as biological systems, geological processes, and engineering applications. In living organisms, it is critical to maintain the right temperature for survival. Animals and humans have evolved mechanisms to regulate body temperature by dissipating excess heat through process like sweating. In electronics field, efficient heat removal is essential for the reliable operation of electronic devices. Modern electronic devices, such as high-performance CPUs and GPUs, generate significant amount of heat due to greater processing power and compact design. If this heat is not dissipated away, it can lead to overheating, reduced performance, and damage to the electronic components. Heat sinks, fans,

\* Corresponding author.

E-mail address: [azwadi@utm.my](mailto:azwadi@utm.my) (Nor Azwadi Che Sidik)

<https://doi.org/10.37934/arnht.15.1.123>

and cooling systems are needed to ensure the electronic components operate within the safe temperature ranges.

Recent advancements in microscale electronic systems, very-large scale integration (VLSI) technologies, aerospace and aviation, and autonomous vehicles, along with miniaturisation of electronic devices, have resulted in substantial increment in the packing densities and heat fluxes generation within these devices. The miniaturisation of electronic devices such as those found in avionics and advanced military equipment are expected to reach 500 to 1000 W/cm<sup>2</sup> [1]. The dramatic increase in heat flux is beyond the capability of many existing heat removal technologies. Efficient thermal management issues have become the most challenging task, demanding immediate concerted attention to address the escalating heat flux. This ensures that there is no limiting barrier for further development of high-density electronics devices, enabling continuous evolution of technology in various sectors.

Moore's Law states that the number of transistors on an integrated circuit would double every eighteen months [2]. The number of semiconductor components on a silicon chip is on exponential rise, and this trend is expected to persist until uncertain limits have been reached. Today, one processor has reached a packing density of billions of transistors over 1 cm<sup>2</sup> area [3]. The continuous increase in transistors density has led to escalation in the amount of heat generated within these devices. The rapid increase in the number of transistors challenges the packaging technology, especially thermal management. The development of next generation heat exchangers is essential to keep pace with the increasing heat flux by modern integrated circuits. Research on improving the efficiency of heat transfer system is ongoing worldwide to develop economically viable solutions for addressing the upcoming heat removal challenges.

Numerous cooling schemes have been proposed to enhance the cooling technology for electronic equipment with high heat generation. The cooling schemes can be categorised into two approaches [4-6]. The first is to optimise the design of cooling devices to maximise their cooling performance. For instance, Samadi *et al.*, [7] simultaneously investigated the cross section, depth, and position of horizontal groove as well as vertical groove to optimise the geometrical parameters in a mini-channel heat sink. After optimisation procedure, they found that the channel base temperature and thermal resistance reduces by 11.8K and 27%, respectively. In another study, Ge *et al.*, [8] applied multi-objective genetic algorithm (MOGA) and particle swarm optimisation (PSO) to optimise the performance of mini-channel heat sink. The optimised cross-sectional shape further reduces the thermal resistance and pumping power by 7.47% and 31.54%, respectively.

The second is to reduce the characteristic length to increase the heat transfer coefficient. The heat transfer coefficient is given by the equation,  $h = k_f Nu/D$ , where  $k_f$  is the thermal conductivity of the coolant,  $Nu$  is the Nusselt number, and  $D$  is the characteristic length. The only way to significantly increase  $h$  for a specific coolant fluid is by reducing  $D$ . Based on the second approach, Tuckerman and Pease [9] designed a high-performance heat sink with channels of microscopic width. Interestingly, scaling the heat exchanger technology to microscopic dimensions increases the surface area to volume ratio up to a significant extent and reduces the convective heat transfer thermal resistance. The higher heat transfer coefficient, together with higher surface area per unit volume, results in maximum thermal resistance of 0.09°C/W over 1 cm<sup>2</sup> area, and heat flux dissipation as high as 790 W/cm<sup>2</sup>.

Since the advent of micro-sized channel heat sinks in 1980s, thermal management of heat transfer systems has undergone a significant shift and transformation. Micro-sized heat sinks have replaced traditional heat sinks in situations where high heat loads cannot be effectively dissipated using traditional methods. The advantage of microchannel lies in their outstanding heat transfer performance and ability to shrink its size for usage in heat exchanger systems. Other advantages

include reduced weight, lower coolant requirements, and reduced use of materials. Microchannels have wide areas of applications in highly specialised fields, such as microfluidic systems, micropumps, and micro-heat pipes. When microchannels are properly designed and utilised, it can distribute the flow precisely, reduced flow length, and establish laminar flow in the channels to reduce the overall pressure drops.

In parallel microchannel, there is a significant variation in the wall temperature along the flow direction due to thickening of the thermal boundary layer [10]. The increased thickness of the boundary layer has a detrimental impact on the effectiveness of heat transfer. Besides that, the effectiveness of heat transfer in a straight microchannel is significantly hindered due to inadequate fluid mixing. Insufficient fluid mixing prevents the fluid from effectively carrying away the generated heat from the channel walls. Due to limited heat dissipation capabilities, the traditional design of microchannel with straight channel is insufficient for accommodating the ongoing advancements in electronic technology. Therefore, a wide range of techniques have been proposed to enhance the heat transfer performance of microchannel. This includes geometrical modification, utilising new class heat transfer fluids, and surface modification [11-15].

Modifications to microchannels include alterations in their cross-sectional shape, aspect ratio, size, as well as adjustments in surface roughness. Additionally, enhancements such as ribs, grooves, and secondary channels are common techniques employed to improve thermal performance of microchannel. Microchannel can be constructed into various shapes, such as rectangular, circular, triangular, and trapezoidal shape. The first work on investigation of new concept microchannels with various shape was numerically studied by Perret *et al.*, [16] in 1998. Their results indicated that rectangular structure presents the lowest thermal resistance compared with diamond and hexagonal structure. In another study, Wang *et al.*, [17] investigated numerically the influence of geometric parameters on flow and heat transfer of microchannel. They observed that, for the same cross-sectional area, rectangular microchannel with higher aspect ratios had a lower thermal resistance.

In another study, Chai *et al.*, [17] conducted a numerical investigation to examine the thermal and hydraulic performance of microchannels with offset ribs on sidewalls. Five different shapes of offset ribs were designed, comprising of rectangular, forward triangular, backward triangular, isosceles triangular, and semi-circular. They found that microchannel with ribs can significantly enhance the heat transfer through the creation of vortices and recirculation flows that interrupt the formation of boundary layers. The results showed that microchannel with forward triangular offset ribs achieved the highest performance for Reynolds number lesser than 350. On the other hand, the microchannel with semi-circular offset ribs yielded the best performance for Reynolds number higher than 400. The overall performance of microchannel is ranged between 1.02 to 1.48 compared to the simple rectangular microchannel.

Lee *et al.*, [18] proposed a new concept of microchannel with openings in the form of oblique cuts to create smaller branching channels along the flow direction. The introduction of oblique fins in microchannel results in disruption and subsequent re-initialisation of boundary layers at each passage and generation of secondary flows. The combined effect of oblique fins results in a remarkable enhancement in heat transfer with minimal pressure drop. In a similar study, Kuppusamy *et al.*, [19] numerically studied a microchannel with slanted secondary passage in alternating orientation. Introducing intervallic secondary passages offer numerous advantages, including the disruption and redevelopment of the hydrodynamic boundary layer, along with enhanced flow mixing. The optimised design resulted in a 146% increase in overall performance and 76.8% decrease in thermal resistance compared to the simple microchannel.

In a related research, Ghani *et al.*, [20] proposed a novel microchannel with secondary oblique channels and rectangular ribs. The proposed design reduced the pressure drop caused by ribs alone

by 50%. The hybrid microchannel design increased chaotic advection and flow mixing, which improved the cooling performance of microchannel. Based on the review of the literature, the enhancements such as ribs and secondary channels can enhance the thermal performance of microchannel. However, to the author's best knowledge, there is no research that have been done combining secondary channels and ribs with tertiary channels. Therefore, the aim of present study is to present a new design that exploits the characteristics of secondary channels which provide larger flow area to reduce the pressure drop caused by ribs. In the new design, the ribs are positioned further away from the channel centre, which results in a decrease in heat transfer efficiency and pressure drop. To counteract this effect, tertiary channels are introduced to improve the heat transfer.

## 2. Methodology

### 2.1 Model Description for Microchannel Heat Sink

The microchannel heat sink consists of an array of channels, and the number of channels constructed depends on the area of application. To reduce computational effort and take advantage of the symmetry boundary conditions, only one symmetrical part of the microchannel is adopted for numerical simulation. Figure 1-5 show the computational domain of conventional rectangular microchannel (MC-RC), microchannel with rectangular ribs (MC-RR), microchannel with secondary channels (MC-SC), microchannel with secondary channels and rectangular ribs (MC-SC-RR), and microchannel with secondary channels and tertiary channels and rectangular ribs (MC-SC-TC-RR). The main dimensions of the microchannel such as length, width, and height is 10 mm, 0.25 mm, and 0.35 mm, respectively. The detail geometrical parameters of all microchannel are given in Table 1.

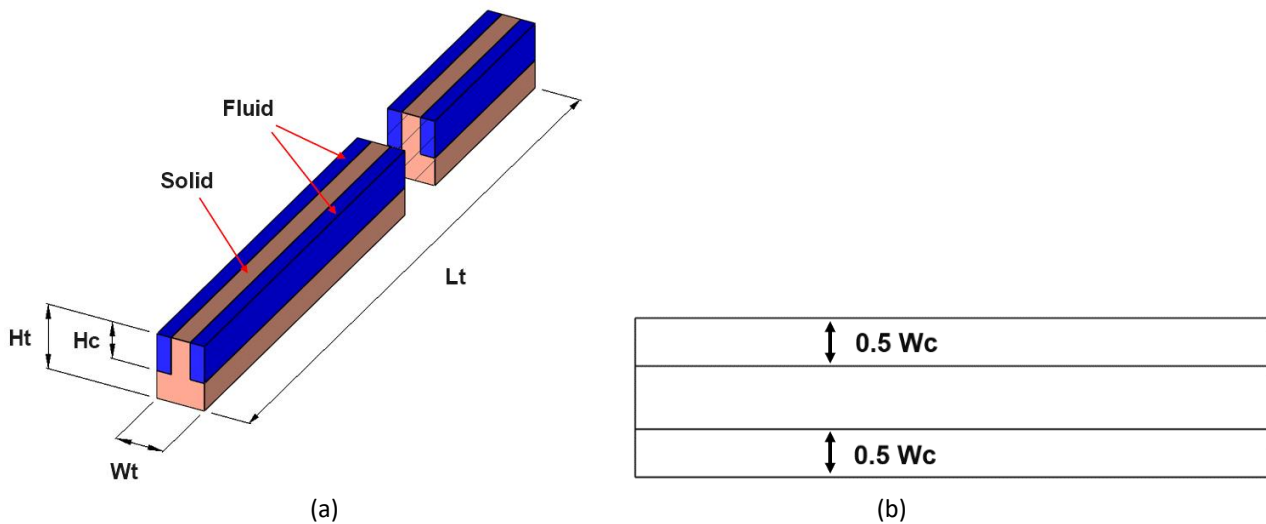


**Fig. 1.** (a) Schematic diagram of MC-RC (b) Geometric parameters of MC-RC

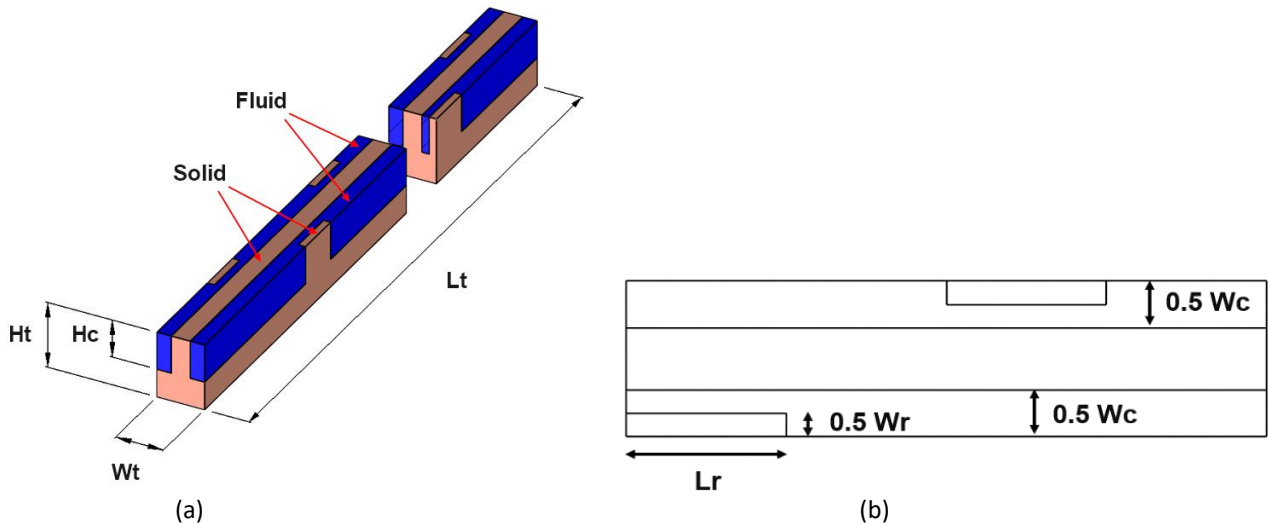


**Fig. 2.** (a) Schematic diagram of MC-RR (b) Geometric parameters of MC-RR

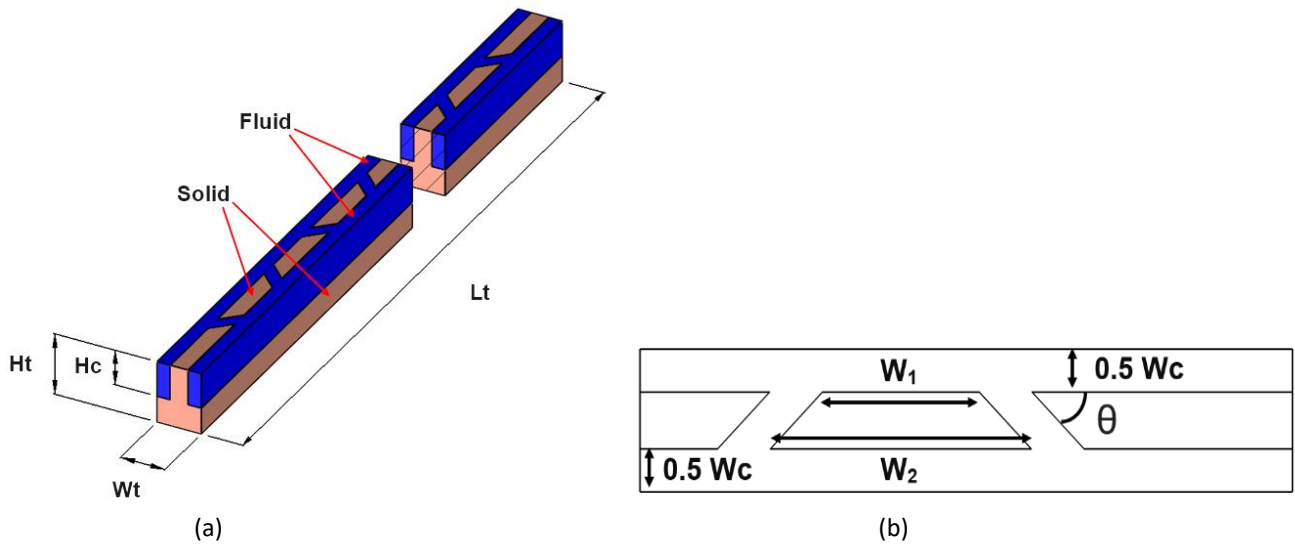


**Fig. 3.** (a) Schematic diagram of MC-SC (b) Geometric parameters of MC-SC

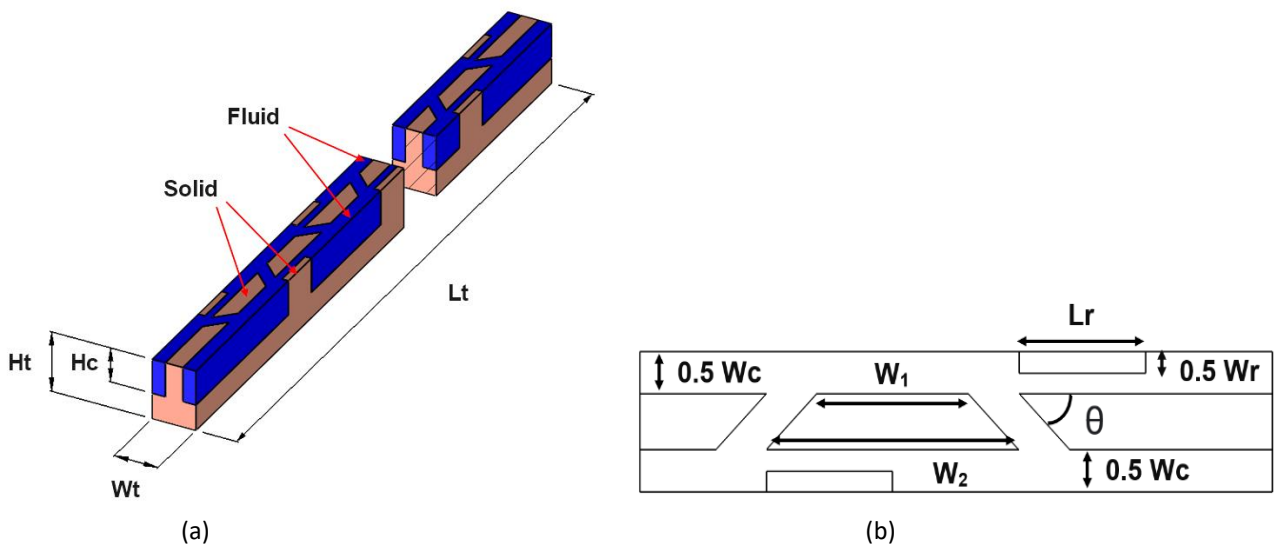


**Fig. 4.** (a) Schematic diagram of MC-SC-RR (b) Geometric parameters of MC-SC-RR

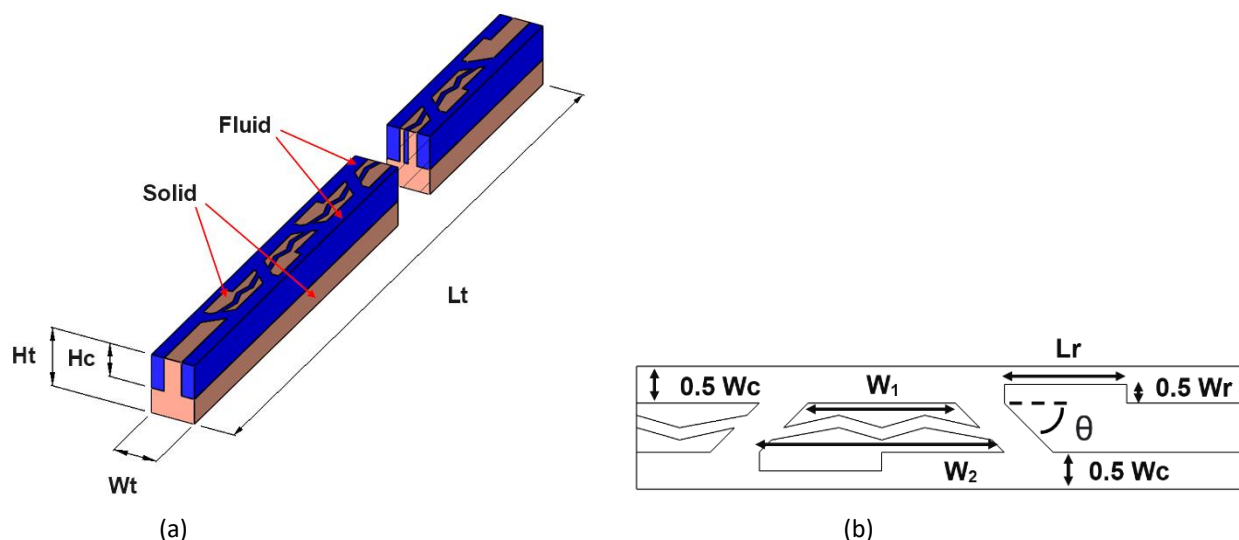


**Fig. 5.** (a) Schematic diagram of MC-SC-TC-RR (b) Geometric parameters of MC-SC-TC-RR

**Table 1**

Geometrical parameters of MCHS

Geometrical parameters	Value
Ht	35 $\mu\text{m}$
Hc	20 $\mu\text{m}$
Lt	10,000 $\mu\text{m}$
Wt	25 $\mu\text{m}$
Wc	15 $\mu\text{m}$
Lr	25 $\mu\text{m}$
Wr	75 $\mu\text{m}$
W <sub>1</sub>	30 $\mu\text{m}$
W <sub>2</sub>	50 $\mu\text{m}$
W <sub>sc</sub>	50 $\mu\text{m}$
$\theta$	45°

## 2.2 Numerical Method

Numerical simulation is performed using commercial computational fluid dynamics (CFD) software ANSYS FLUENT 17.0 to solve the three-dimensional fluid flow and heat transfer governing equations according to the following assumptions.

- i. The flow is assumed steady state, incompressible and laminar.
- ii. The working fluid used in the study is water.
- iii. The fluid properties are assumed varied according to the temperature.
- iv. The solid properties are assumed constant.
- v. The viscous dissipation and the gravitational force have negligible effect.
- vi. The radiation heat transfer is neglected.
- vii. The wall is assumed adiabatic where heat is not allowed to dissipate from the wall.
- viii. A uniform heat flux is applied at the bottom of the wall to replicate the heat generated by thermal device.
- ix. Due to symmetrical geometry, only one single channel is used for numerical simulation.

### 2.2.1 Governing equations

Continuity equation

$$\frac{\partial u}{\partial x} + \frac{\partial v}{\partial y} + \frac{\partial w}{\partial z} = 0 \quad (1)$$

Where the components  $u$ ,  $v$ , and  $w$  represent the velocity in  $x$ ,  $y$ , and  $z$  direction respectively.

Momentum equations

$$u \frac{\partial u}{\partial x} + v \frac{\partial u}{\partial y} + w \frac{\partial u}{\partial z} = -\frac{1}{\rho_f} \frac{\partial \rho}{\partial x} + \frac{\mu_f}{\rho_f} \left( \frac{\partial^2 u}{\partial x^2} + \frac{\partial^2 u}{\partial y^2} + \frac{\partial^2 u}{\partial z^2} \right) \quad (2)$$

$$u \frac{\partial v}{\partial x} + v \frac{\partial v}{\partial y} + w \frac{\partial v}{\partial z} = -\frac{1}{\rho_f} \frac{\partial \rho}{\partial y} + \frac{\mu_f}{\rho_f} \left( \frac{\partial^2 v}{\partial x^2} + \frac{\partial^2 v}{\partial y^2} + \frac{\partial^2 v}{\partial z^2} \right) \quad (3)$$

$$u \frac{\partial w}{\partial x} + v \frac{\partial w}{\partial y} + w \frac{\partial w}{\partial z} = -\frac{1}{\rho_f} \frac{\partial \rho}{\partial z} + \frac{\mu_f}{\rho_f} \left( \frac{\partial^2 w}{\partial x^2} + \frac{\partial^2 w}{\partial y^2} + \frac{\partial^2 w}{\partial z^2} \right) \quad (4)$$

Where  $\rho_f$ ,  $\mu_f$ , and  $\rho$  represent the density of fluid, dynamic viscosity of fluid, and pressure of fluid.

Energy equation for solid region

$$k_s \left( \frac{\partial^2 T_s}{\partial x^2} + \frac{\partial^2 T_s}{\partial y^2} + \frac{\partial^2 T_s}{\partial z^2} \right) = 0 \quad (5)$$

Where  $k_s$  and  $T_s$  represent the thermal conductivity of solid substrate and temperature of solid substrate.

Energy equation for fluid region

$$u \frac{\partial T_f}{\partial x} + v \frac{\partial T_f}{\partial y} + w \frac{\partial T_f}{\partial z} = \frac{k_f}{\rho_f c_{\rho f}} \left( \frac{\partial^2 T_s}{\partial x^2} + \frac{\partial^2 T_s}{\partial y^2} + \frac{\partial^2 T_s}{\partial z^2} \right) = 0 \quad (6)$$

Where  $T_f$ ,  $k_f$ , and  $c_{\rho f}$  represent the temperature of fluid, thermal conductivity of fluid, and specific heat capacity of fluid.

### 2.2.2 Boundary conditions

Boundary conditions and initial conditions for the present model are given in Table 2. A uniform velocity of 0.5875 to 4.7003 m/s, corresponding to Reynolds number of 100 to 800 are used as the inlet velocity. The inlet temperature of the fluid is set as 293 K. The outlet is set as pressure outlet with zero-gauge pressure (0 atm). The bottom wall of the microchannel is subjected to a uniform heat flux of 100W/cm<sup>2</sup> or 1 × 10<sup>6</sup>W/m<sup>2</sup>. The top solid and fluid wall of the microchannel are set as adiabatic conditions. At the sidewalls, symmetry boundary conditions are applied. At the solid fluid interface, thermal coupled condition is applied to investigate the conjugate heat transfer in the inner wall.

**Table 2**  
Boundary and initial conditions

Boundary	Location	Condition
Thermal	At inlet, x = 0 mm	$T_f = T_{in} = 293K$ (fluid) $-k_s \left( \frac{\partial T_s}{\partial x} \right) = 0$ (solid)
	At outlet, x = 10 mm	$-k_f \left( \frac{\partial T_f}{\partial x} \right) = 0$ (fluid) $-k_s \left( \frac{\partial T_s}{\partial x} \right) = 0$ (solid)
	At lower wall, z = 0 mm	$-k_s \left( \frac{\partial T_s}{\partial z} \right) = 100W/cm^2$
	At upper wall, z = 0.35 mm	$-k_s \left( \frac{\partial T_s}{\partial z} \right) = 0$
	At left wall, y = 0 mm	$\frac{\partial}{\partial y} = 0$ (symmetry)
	At right wall, y = 0.25 mm	$\frac{\partial}{\partial y} = 0$ (symmetry)
	Hydrodynamic	At inlet, x = 0 mm
At outlet, x = 10 mm		$p_f = p_{out} = 0$ atm
At solid fluid interface		$u = v = w = 0$ $-k_s \left( \frac{\partial T_s}{\partial n} \right) = -k_f \left( \frac{\partial T_f}{\partial n} \right)$

### 2.2.3 Thermophysical properties

Microchannel substrate is made from copper due to its high thermal conductivity which facilitates heat exchange. The thermophysical properties of copper are listed in Table 3. The working fluid used in microchannel is water due to having relatively high thermal conductivity and heat capacity, making it effective in applications where heat needs to be dissipated away quickly. The thermophysical properties of water depends on temperature in accordance to Incropera [21] as shown in Eq. (1) – Eq. (4).

$$\rho = \frac{999.84 + 18.225(T - 273) - 7.92 \times 10^{-3}(T - 273)^2 - 5.545 \times 10^{-5}(T - 273)^3 + 1.498 \times 10^{-7}(T - 273)^4 - 3.933 \times 10^{-10}(T - 273)^5}{1 + 1.816 \times 10^{-2}(T - 273)} \quad (7)$$

$$\mu = 2.414 \times 10^{-5} \times 10^{\frac{247.8}{T-140}} \quad (8)$$

$$c_p = 8958.9 - 40.535T + 0.11243T^2 - 1.014 \times 10^{-4}T^3 \quad (9)$$

$$k = -0.58166 + 6.3556 \times 10^{-3}T - 7.964 \times 10^{-6}T^2 \quad (10)$$

**Table 3**  
Thermophysical properties of copper

Density (kg/m <sup>3</sup> )	Specific heat (J/kg K)	Thermal conductivity (W/m K)
8978	381	387.6

### 2.2.4 Grid Independence Test (GIT)

Grid independence test has been carried out to find the optimum size of the mesh which produce accurate numerical results with lower computational costs. It is an essential step in numerical simulation to ensure the reliability and accuracy of computational results. The test involves systematically refining and coarsening the computational grid to evaluate its impact on simulation results. Coarse grids create a significant spatial discretisation error, while very fine grids may increase the round-off error which reduces the accuracy of results. By running the simulation with different grid resolutions, it is possible to find the number of grids that is sufficiently fine to capture the relevant fluid flow and heat transfer characteristics accurately. The microchannel is designed using SolidWorks software, and Ansys ICEM software is used to generate structured mesh for the solver. Figure 6-10 show the three-dimensional hexahedral meshes and meshes in the x-y plane for various configurations of MCHS. Hexahedral meshes are used due to faster solution convergence while maintaining high accuracy.

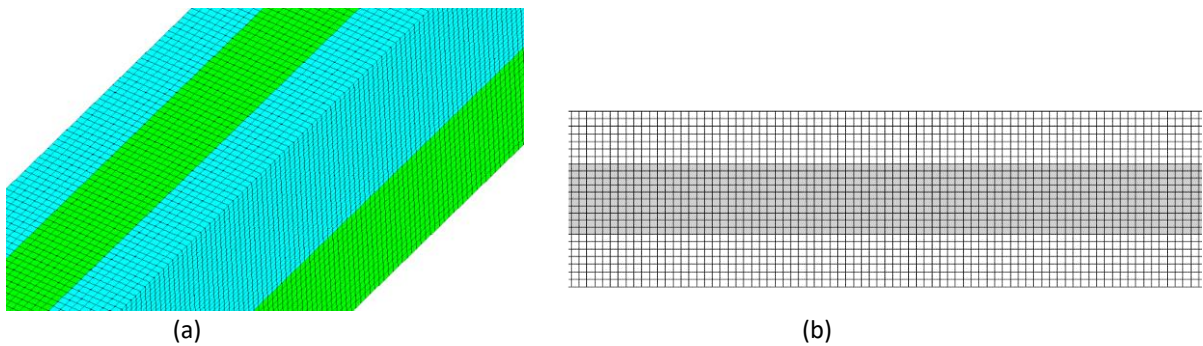


**Fig. 6.** (a) Three-dimensional mesh of MC-RC (b) Mesh in the x-y plane of MC-RC

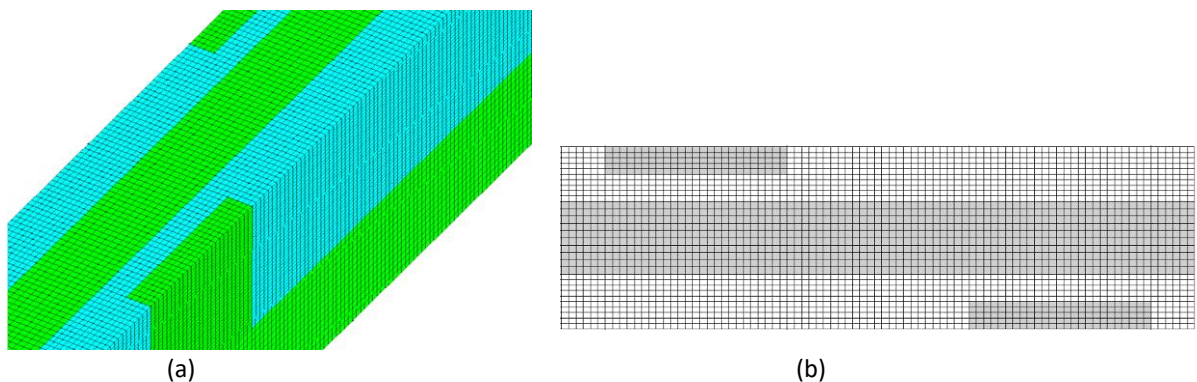


**Fig. 7.** (a) Three-dimensional mesh of MC-RR (b) Mesh in the x-y plane of MC-RR

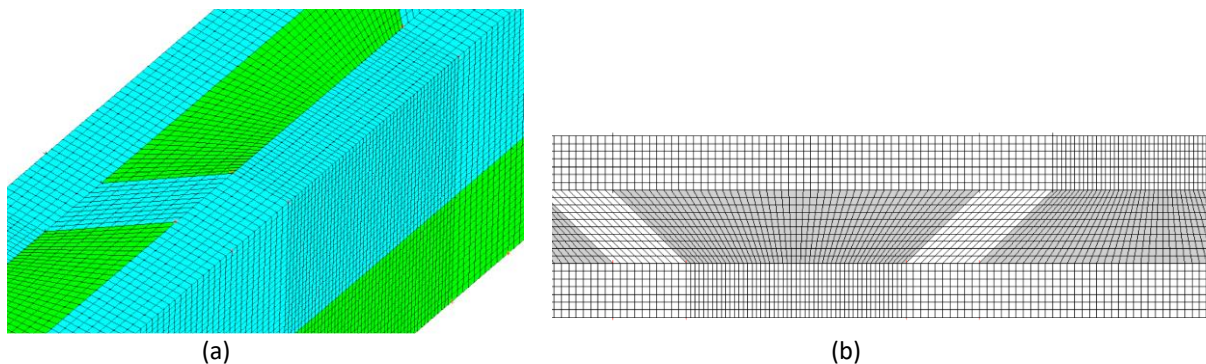


**Fig. 9.** (a) Three-dimensional mesh of MC-SC-RR (b) Mesh in the x-y plane of MC-SC-RR

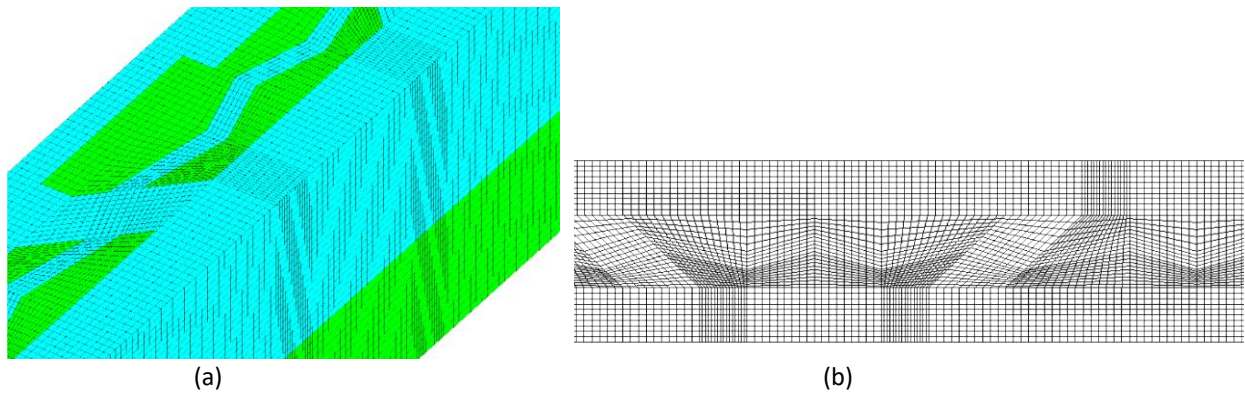


**Fig. 10.** (a) Three-dimensional mesh of MC-SC-TC-RR (b) Mesh in the x-y plane of MC-SC-TC-RR

Mesh generation plays a crucial role in numerical simulations, as it directly impacts the accuracy and computational resources. In the present study, the finest mesh has the highest number of elements, up to 1 million to ensure that the results of simulation independent of mesh size or grid resolution. In addition, the grid independence study focuses on the highest Nusselt number ( $Re = 800$ ). At higher Nusselt numbers, the temperature gradients and fluid flow behaviour become much more pronounced, leading to greater variations in the results obtained with different grid resolutions. Therefore, conducting the simulation study at higher Nusselt number allows for a more rigorous assessment of how mesh resolution affects the accuracy of the results. Six different mesh sizes are generated using ICEM software, ranging from a very fine mesh with high element count to coarser meshes with fewer elements. The relative error is calculated according to following equation:

$$\varepsilon = \left| \frac{J_2 - J_1}{J_1} \right| \times 100\% \quad (11)$$

Where the parameter of interest is denoted by J. It is used to represent performance metrics from numerical simulation, such as Nusselt number, wall temperature, or pressure drop.  $J_1$  represents the parameter value obtained from the finest grid, whereas  $J_2$  represents the parameter value obtained from a coarser grid. Table 4-8 show the relative errors for Nusselt number and pressure drop for various mesh resolutions. These relative errors are expressed as percentages and are computed by comparing the results obtained from coarser meshes to those from the baseline mesh. It is clearly shown that grid number 3 provides a reasonable accuracy for MC-RC, MC-RR, and MC-SC. Meanwhile, grid number 2 offers satisfactory results for MC-SC-RR and MC-SC-TC-RR. Consequently, it is shown that a coarser mesh is adequate for the numerical simulation with deviation of less than 1% compared to the finest mesh.

**Table 4**  
 Grid independency test for MC-RC at  $Re = 800$

No	Number of cells	Nu	$\varepsilon$ (%)	Pressure drop (Pa)	$\varepsilon$ (%)
1	1,200,000	8.2630	-	52660.16	-
2	1,080,000	8.2677	0.0568	52595.37	0.1230
3	960,000	8.2759	0.1559	52501.14	0.3020
4	840,000	8.2913	0.3426	52354.12	0.5812
5	600,000	8.2909	0.3381	52354.18	0.5810
6	360,000	8.3798	1.4142	51386.66	2.4183

**Table 5**  
 Grid independency test for MC-RR at Re = 800

No	Number of cells	Nu	$\varepsilon$ (%)	Pressure drop (Pa)	$\varepsilon$ (%)
1	1,650,000	24.3004	-	538518.40	-
2	1,500,000	24.3077	0.0298	537085.80	0.2660
3	1,350,000	24.3123	0.0489	536934.50	0.2941
4	1,200,000	24.9037	2.4826	554866.50	3.0358
5	1,050,000	25.5571	5.1714	582575.80	8.1812
6	810,000	25.5474	5.1315	582569.10	8.1800

**Table 6**  
 Grid independency test for MC-SC at Re = 800

No	Number of cells	Nu	$\varepsilon$ (%)	Pressure drop (Pa)	$\varepsilon$ (%)
1	1,285,200	7.7295	-	51507.72	-
2	1,142,400	7.6835	0.5950	51404.37	0.2006
3	999,600	7.7063	0.3003	51246.03	0.5081
4	856,800	7.7612	0.4098	50971.64	1.0408
5	714,000	7.8574	1.6550	50313.70	2.3181
6	571,200	7.6586	0.9175	46917.54	8.9116

**Table 7**  
 Grid independency test for MC-SC-RR at Re = 800

No	Number of cells	Nu	$\varepsilon$ (%)	Pressure drop (Pa)	$\varepsilon$ (%)
1	1,606,500	30.3450	-	417945.00	-
2	1,428,000	30.1460	0.6559	418025.40	0.0192
3	1,249,500	29.4929	2.8080	421156.50	0.7684
4	1,071,000	28.2435	6.9256	411943.90	1.4359
5	892,500	26.6094	12.3105	378061.60	9.5427
6	714,000	24.3576	19.7312	338436.40	19.0237

**Table 8**  
 Grid independency test for MC-SC-TC-RR at Re = 800

No	Number of cells	Nu	$\varepsilon$ (%)	Pressure drop (Pa)	$\varepsilon$ (%)
1	2,142,000	24.3036	-	253447.7	-
2	1,904,000	24.1472	0.6437	252802.7	0.2545
3	1,666,000	24.9032	2.46695	262816.7	3.6966
4	1,428,000	24.9969	2.8523	264663.6	4.4253
5	1,190,000	23.0829	5.02304	232710.4	8.1821
6	952,000	11.9399	50.8721	150441.3	40.6421

### 2.2.5 Solution algorithm

The numerical simulation is performed using computational fluid dynamics (CFD) method to study the fluid flow and heat transfer in microchannel. The numerical solver solves the governing equations based on conservation law for the heat and mass transfer and fluid flow to achieve the results. The governing equations for conservation law are continuity equation, momentum equation, and energy equation. The discretisation of the domain is based on finite volume method. Since the fluid is incompressible, pressure-based solver is selected. The laminar flow model is selected for simulation of flow with Reynolds number less than 2300. COUPLED scheme is used to determine the pressure

and velocity field. The upwind scheme is selected as second order for pressure, momentum, and energy equation. The gradient used to discrete the flow conservation equation is least squared cell based. The solution is converged when the residual of energy, continuity value is less than  $10^{-6}$ .

### 2.2.6 Data reduction

The Reynolds number is given as

$$Re = \frac{\rho_f u_m D_h}{\mu} \quad (12)$$

Where  $\rho_f$ ,  $u_m$ ,  $D_h$  and  $\mu$  represent the density of fluid, mean velocity of fluid, hydraulic diameter of channel, and dynamic viscosity, respectively.

The hydraulic diameter of microchannel is calculated as

$$D_h = \frac{2H_c W_c}{H_c + W_c} \quad (13)$$

Where  $H_c$  and  $W_c$  represent the height of the channel and width of the channel respectively.

The average apparent friction factor is calculated as

$$f_{app,ave} = \frac{2D_h \Delta P}{L_t \rho u_m^2} \quad (14)$$

$$\Delta P = P_{in} - P_{out} \quad (15)$$

Where  $\Delta P$  and  $L_t$  represent the change in pressure between inlet and outlet section and total length of the microchannel.

The average heat transfer coefficient is given as

$$h_{ave} = \frac{\dot{q}_w}{T_{w,ave} - T_{bulk,ave}} \quad (16)$$

$$T_{w,ave} = \frac{\int T dA}{\int dA} \quad (17)$$

$$T_{bulk,ave} = \frac{\int \rho \mu C_p T dA}{\int \rho \mu C_p dA} \quad (18)$$

Where  $\dot{q}_w$ ,  $T_{w,ave}$  and  $T_{bulk,ave}$  represent the heat flux at the lower wall of microchannel, average wall temperature in the solid fluid interface (conjugate area), and average bulk fluid temperature, respectively.

The average Nusselt number is calculated as

$$Nu_{ave} = \frac{h_{ave} D_h}{k_f} \quad (19)$$

Where  $k_f$  represent the thermal conductivity of fluid.

The total thermal resistance is calculated as

$$R_{th} = \frac{T_{w,max} - T_{in}}{Q} \quad (20)$$

Where  $T_{w,max}$ ,  $T_{in}$  and  $Q$  represent the maximum wall temperature, fluid inlet temperature, and total heat supplied to the system.

### 3. Results and Discussion

#### 3.1 Validation of Rectangular Microchannel Heat Sink using Empirical Correlations

To ensure that numerical simulation results are accurate, they must be validated against experimental data or empirical correlations. It is a general practice to simplify the geometry and boundary conditions to reduce the computational complexity. Excessive simplification of the geometry and boundary conditions can lead to inaccurate numerical results. In addition, numerical validation is also essential to demonstrate that the same numerical procedure can be applied to different geometric configurations and parameters. To assess the accuracy of the numerical simulations, local Nusselt number, apparent friction factor, and pressure drop for rectangular microchannel (MC-RC) are validated with correlations. The correlations of Philips have been used to acquire the theoretical results for local Nusselt number and Steinke & Kandlikar are used for apparent friction factor, and pressure drop [22,23].

The local Nusselt number for three sides heating microchannels is given by

$$Nu_x = Nu_{x,3} = Nu_{x,4} \left( \frac{Nu_{fd,3}}{Nu_{fd,4}} \right) \quad (21)$$

where  $Nu_{fd,3}$  and  $Nu_{fd,4}$  refer to the Nusselt numbers for the three-sided and four-sided heating cases in fully developed laminar flow.

$$Nu_{x,4} = \frac{28.315 + 27038(x^*) + 1783300(x^*)^2}{1 + 3049(x^*) + 472520(x^*)^2 - 35714(x^*)^3} \quad (22)$$

$$x^* = \frac{x}{D_h Re Pr} \quad (23)$$

$$Nu_{fd,3} = \frac{8.2321 + 2.0263(\alpha) + 1.2771(\alpha)^2}{1 + 0.29805(\alpha) + 2.2389(\alpha)^2 + 0.0065322(\alpha)^3} \quad (24)$$

$$Nu_{fd,4} = \frac{8.2313 + 1.9349(\alpha) - 2.295(\alpha)^2}{1 + 0.92381(\alpha) + 7.928(\alpha)^2 + 0.0033937(\alpha)^3} \quad (25)$$

$$\alpha = \frac{W_c}{H_c} \quad (26)$$

Where  $\alpha$ ,  $W_c$  and  $H_c$  refer to the channel aspect ratio, width of microchannel, and height of microchannel, respectively.

The friction factor in the developing region is predicted by

$$f_{app} = f + \frac{H(\alpha)D_h}{L_t} \quad (27)$$

Where  $f_{app}$  and  $H(\alpha)$  represent the apparent friction factor accounting for developing region, and Hagenbach's factor.

The Poiseuille number is written as

$$Po = fRe = 96(1 - 1.3553\alpha + 1.9467\alpha^2 - 1.7012\alpha^3 + 0.9564\alpha^4 - 0.2537\alpha^5) \quad (28)$$

Where  $\alpha$  is the channel aspect ratio.

The Hagenbach's factor is related to aspect ratio by

$$H(\alpha) = 0.6796 + 1.2197\alpha + 3.3089\alpha^2 - 9.5921\alpha^3 + 8.9089\alpha^4 - 2.9959\alpha^5 \quad (29)$$

The corresponding pressure drop then becomes

$$\Delta p = \frac{2(fRe)\mu u_m L_t}{D_h} + \frac{H(\alpha)\rho u_m^2}{2} \quad (30)$$

Figure 11 illustrates the comparison between numerical simulation results and theoretical calculation results of local Nusselt number, apparent friction factor, and pressure drop. The results obtained from numerical simulation and empirical correlation show similar trends. The

Local Nusselt number decreases as the non-dimensional distance increases. The pressure drop increases and apparent friction factor decreases as Reynolds number increases. Additionally, the mean average error is computed, and the maximum deviation of the results are 6.82%, 6.75%, and 3.18% for local Nusselt number, pressure drop, and apparent friction factor. It is clearly shown that the results of numerical simulations are in good agreement with empirical correlations. This agreement indicates that the current numerical simulation method can be used to predict the fluid flow and heat transfer behaviour in other MCHS.

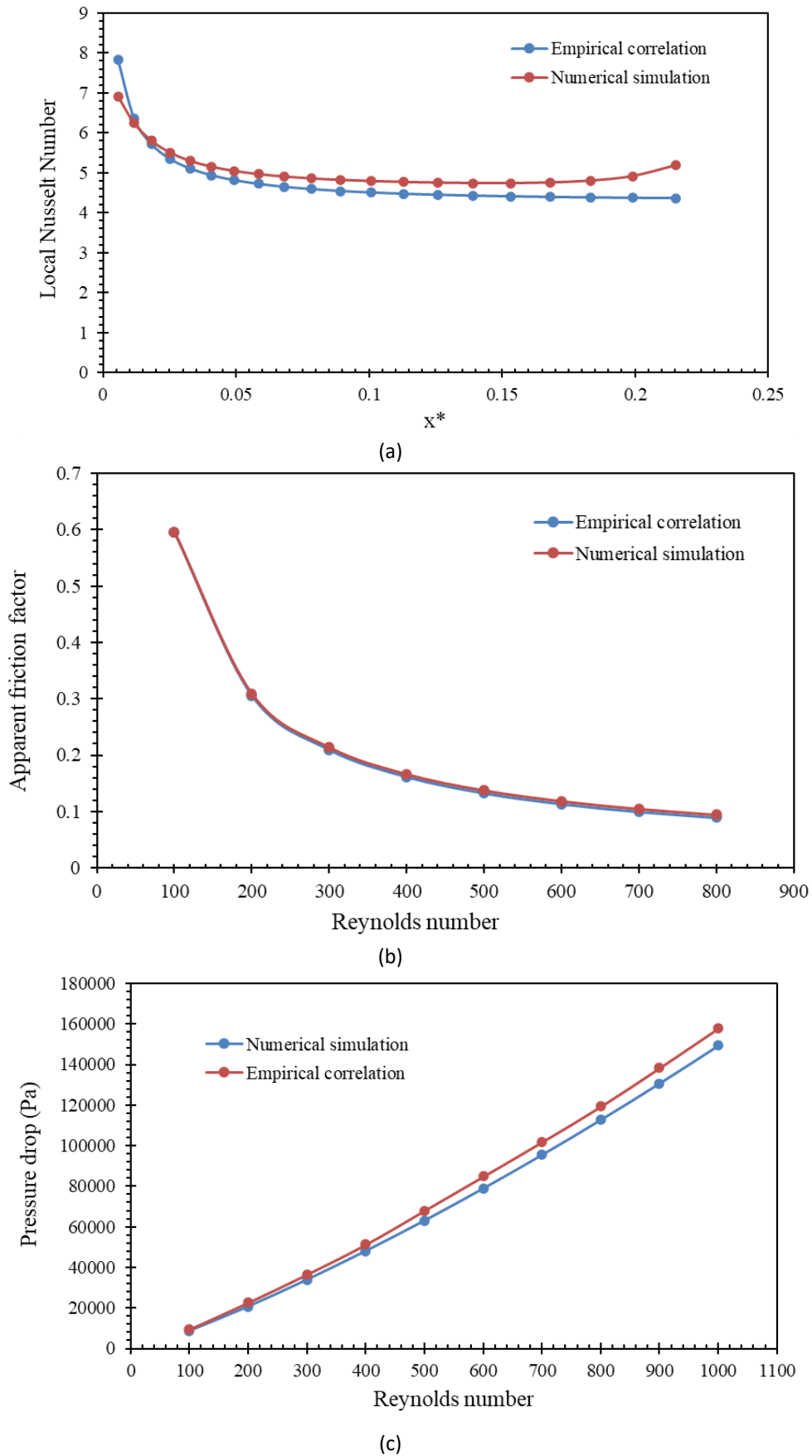


**Fig. 11.** Numerical validation of (a) local Nusselt number according to Philips [22] (b) apparent friction factor according to Steinke & Kandlikar [23] and (b) pressure drop according to Steinke & Kandlikar [23]

### *3.2 Fluid Flow and Heat Transfer Characteristics of Microchannel Heat Sink with Different Geometry Structures*

#### *3.2.1 Effect of geometry structures on velocity distribution*

To analyse the effects of different geometry structures on the fluid flow characteristics in microchannel heat sink, a comparative study has been conducted to investigate the geometry structures under identical Reynolds number conditions ( $Re = 300$ ) on x-y plane at  $z = 0.25$  mm. Figure 12 illustrates the velocity contour plots and flow streamlines distributions of various configurations of MCHS. The flow streamlines visualisation helps to identify the zones that promote flow separation, flow recirculation, and eddy formation. The velocity contour plot contributes to assessing the uniformity of fluid flow and regions of high and low velocities. The geometry structures used are rectangular microchannel (MC-RC), microchannel with rectangular ribs (MC-RR), microchannel with secondary channels (MC-SC), microchannel with secondary channels and rectangular ribs (MC-SC-RR), and microchannel with secondary channels and tertiary channels and rectangular ribs (MC-SC-TC-RR).

In MC-RC, the flow streamlines are parallel to each other without any deviations. In MC-RR, the presence of rectangular shaped ribs as obstacles has led to complex and altered flow patterns. The smooth flow of fluid is disrupted by the ribs, and the flow streamlines are forced to deviate from its original path and change its trajectory to flow into the gap between the channel walls. As the fluid flows out of the narrow gap between the channel walls, due to sudden changes in the channel cross-section, flow streamlines at the downstream of the ribs formed vortices or recirculation zones. In MC-SC, the flow streamlines exhibit unique pattern due to presence of interconnected channels. The flow streamlines are closely similar to those found in MC-RC, except that some of the flows are slightly deviated towards the secondary channels.

In MC-SC-RR, the hybrid design of microchannel having ribs and secondary channels has a different influence on the flow behaviour. The ribs cause extra flow streamlines to periodically move from one primary channel to adjacent primary channel through the secondary channels. In the absence of ribs, the flow streamlines are less likely to move into the secondary channels.

The main reason for this behaviour is that the primary channel has no physical obstructions to redirect and guide the fluid flow. In MC-SC-TC-RR, the flow streamlines exhibit intricate and controlled behaviour due to presence of multiple geometry features that influence the flow. Rectangular shaped ribs positioned along the sidewalls of the channels introduce sufficient disturbance to the main flow within the primary channel. This causes the flow streamlines to be redistributed into secondary and tertiary channels evenly.

Velocity contour plot for MC-RC reveals a parabolic velocity distribution along the channel length. The fluid velocity reaches its maximum at the channel centre, gradually diminishing as it approaches the channel walls. A closely similar flow behaviour is noticed in MC-SC, except that the minimum flow velocity is found inside the secondary channels. A different velocity distribution is observed in MC-RR where the maximum velocity is observed at the sidewalls of ribs and minimum velocity is found behind the ribs. The highest velocity appears in adjacent to sidewalls due to narrow flow passage which cause fluid to accelerate. The lowest velocity found behind the ribs due to recirculating flow. In MC-SC-RR, the maximum velocity is located at the sidewalls of ribs and frontal region of ribs due to flow gathering zone and minimum velocity is witnessed behind the ribs. In MC-SC-TC-RR, the maximum velocity is observed near the channel centre due to narrow flow passage and minimum velocity behind the ribs.

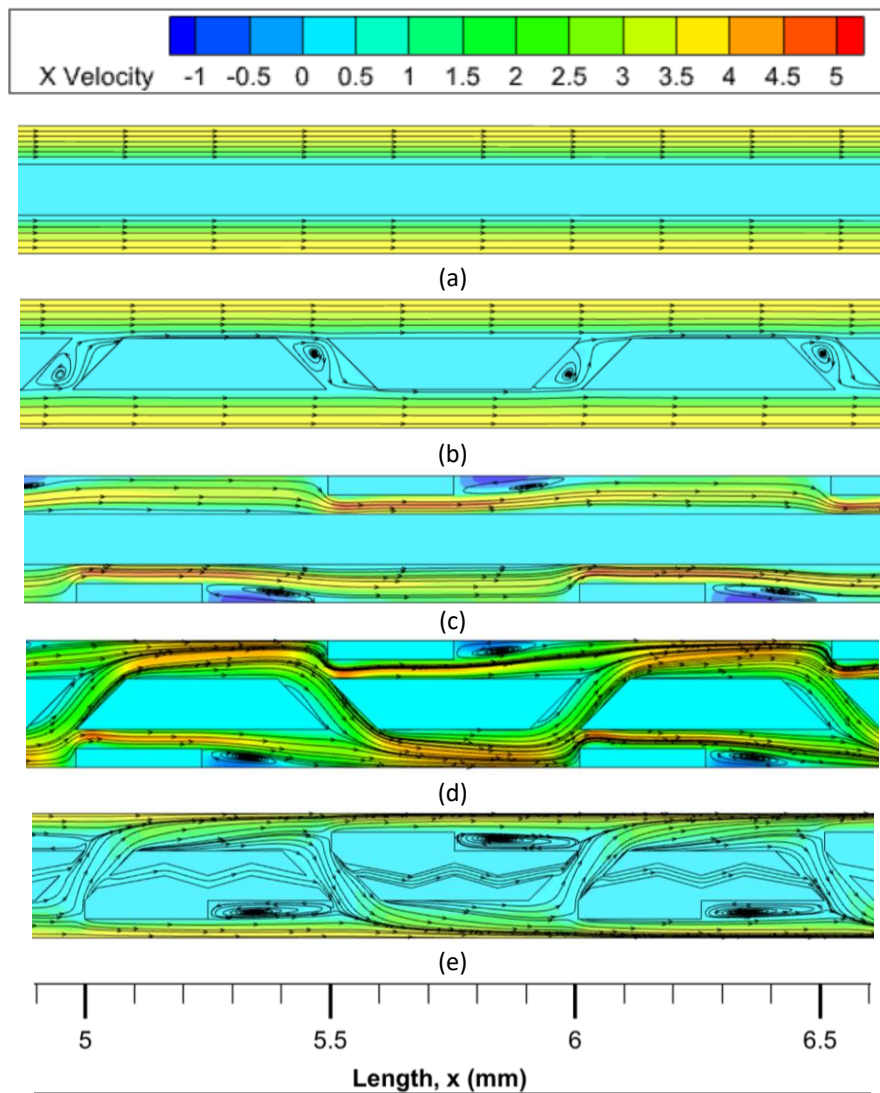


**Fig. 12.** Streamlines and velocity distribution on x-y plane ( $z = 0.25$  mm) at  $Re = 300$  for (a) MC-RC (b) MC-SC (c) MC-RR (d) MC-SC-RR (e) MC-SC-TC-RR

### 3.2.2 Effect of geometry structures on pressure distribution

The pressure distributions of different microchannel heat sink are shown in Figure 13. For all cases studied, it is found that the upstream pressure is always higher than the downstream pressure, with the pressure gradually decreases until reaching zero at the channel exit. When pressure decreases along the flow, it denotes that pressure drop occurs within the channel. In MC-RC, the static pressure decreases steadily along the flow channel due to frictional and energy losses. In addition, it is found that the pressure drop trend in MC-SC closely resembles that of MC-RC. The pressure drops in these channels are impressively lower due to straight and free of flow obstructing geometries. Among all the configurations, MC-SC exhibits the lowest pressure drop. This is attributed to the local pressure recovery effect provided by the secondary channels, which offsets the increase in pressure drop [24].

The pressure drop in MC-RR is the highest in comparison to other geometry configurations. The existence of ribs has a considerable effect on the pressure drop in microchannel. As the flow reaches the leading edge of the ribs, it experiences an increase in pressure due to the Bernoulli Effect. Conversely, at the downstream of ribs, a region of lower pressure develops as a result of recirculation

flow occurs. The integration of secondary channels with the ribs in configurations like MC-SC-RR has substantially reduced pressure drop. The frictional losses caused by the ribs is reduced to a minimum level due to enlargement of flow area provided by the secondary channel. In MC-SC-TC-RR, the relocation of ribs from the channel centre to the sidewall leads to a notable reduction in static pressure. This is attributed to the weakening of flow blockage intensity associated with such rib alignment.

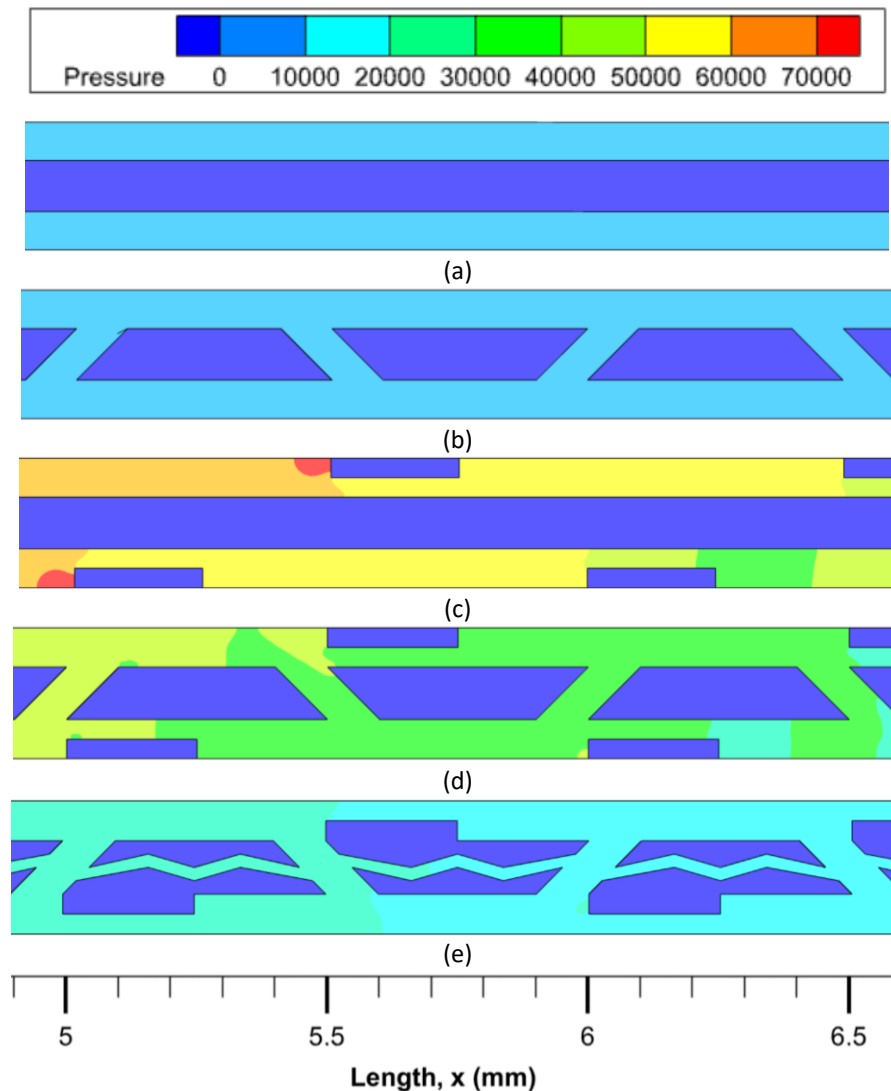


**Fig. 13.** Pressure distribution on x-y plane ( $z = 0.25$  mm) at  $Re = 300$  for (a) MC-RC (b) MC-SC (c) MC-RR (d) MC-SC-RR (e) MC-SC-TC-RR

### 3.2.3 Effect of geometry structures on temperature distribution

Figure 14 shows the two-dimensional temperature contour plots for microchannel with different geometry structures under identical Reynolds number conditions ( $Re = 500$ ) on x-y plane at  $z = 0.25$  mm. Analysis of the contour plots reveals that MC-RC exhibits the highest temperature distribution compared to other structures. It is observed that the temperature undergoes a significant variation along the direction of fluid flow, from 293 K to 322.36 K. The large temperature variation indicates that the heat transfer system cannot be used effectively to dissipate heat. In addition, a steep temperature gradient is observed near the sidewall and centre of the channel. This implies that a

non-uniform temperature distribution exists within the channel. The same trend of temperature distribution is noticed in MC-SC, but it exhibits minor enhancement in the heat transfer performance.

MC-RR displays a temperature distribution that is markedly dissimilar from the two cases examined earlier. There is a noticeable decrease in solid wall temperature, with the highest temperature reaching a value of 305.72 K. This change can be attributed to the introduction of ribs within the microchannel, which enhances the fluid mixing between colder and hotter fluids. The temperature distribution of MC-SC-RR and MC-SC-TC-RR shows the lowest among the others. Incorporating secondary and tertiary channels along with ribs within microchannel has demonstrated greater effectiveness in improving temperature distribution compared to utilising the structures individually. As a result, both solid wall and fluid temperatures exhibit higher uniformity than previous structures. Besides that, the inclusion of additional channels within the microchannel increases the surface area available for heat exchange, which results in a much lower temperature distribution.

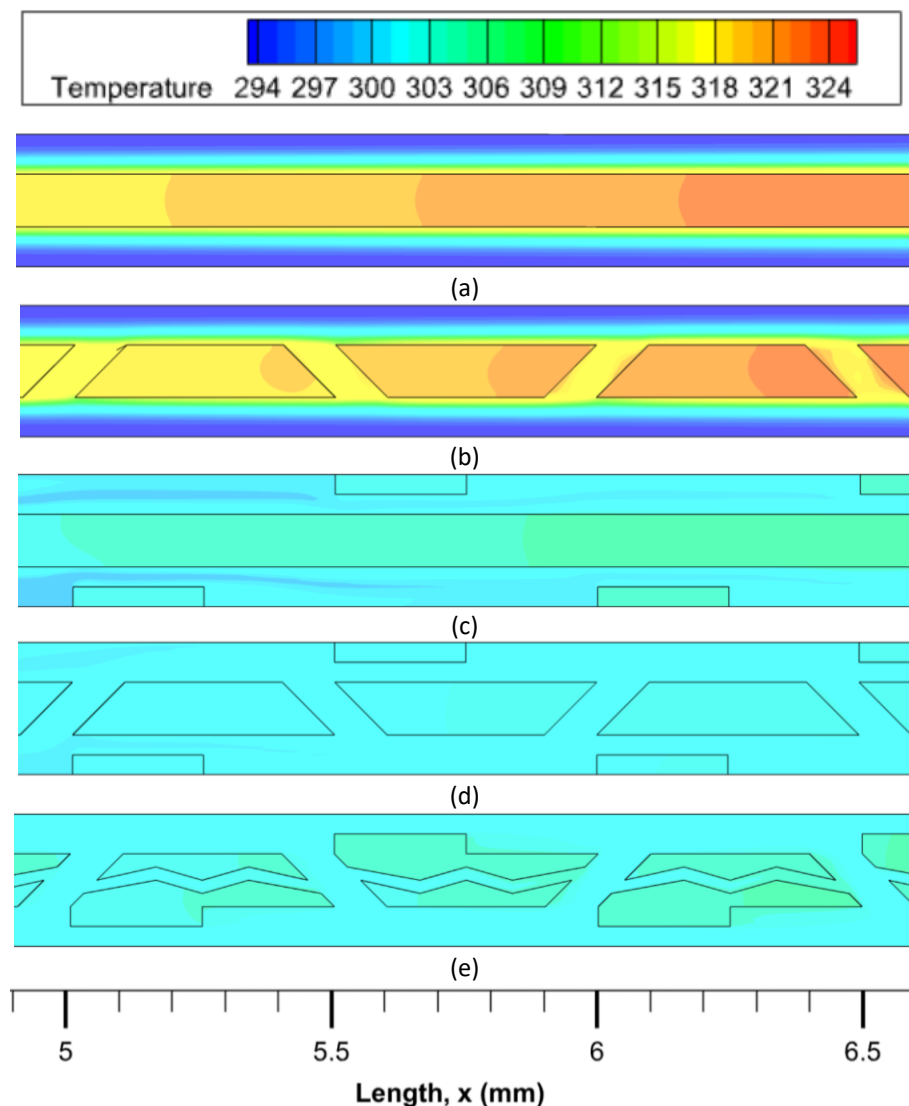


**Fig. 14.** Temperature distribution on x-y plane ( $z = 0.25$  mm) at  $Re = 500$  for (a) MC-RC (b) MC-SC (c) MC-RR (d) MC-SC-RR (e) MC-SC-TC-RR

### 3.3 Performance Analysis

In the design of microchannel heat sink, an ongoing challenge is the need to make decision between achieving high heat transfer efficiency with the trade-off of higher pressure drop or opting for low heat transfer performance with reduced pressure drop. Depending on the area of application, careful decision making is important in ensuring the microchannel design is the most effective and efficient for heat dissipation. Understanding and optimising the trade-offs involved are paramount to the success of microchannel heat sink design. The application of heat transfer enhancement techniques, while promising in improving heat transfer coefficient, often results in an increase in the friction factor and, consequently, higher pressure drop [25]. To arrive at the most effective and efficient microchannel design, rigorous studies are needed to quantify the impacts of different design choices that strike a balance between heat transfer efficiency and pressure drop.

In this study, performance evaluation criteria are established based on the comparison of the thermal resistance among different microchannel configurations. Figure 15 illustrates the variation of total thermal resistance with Reynolds number for various geometry structures. Across all configurations, it is observed that thermal resistance tends to be higher at lower Re and experiences a sharp decrease as Re increases. In the specified range of Reynolds number, MC-SC-RR consistently presents lower thermal resistance in contrast to both conventional and enhanced microchannel designs. However, with increasing Re, the disparity in thermal resistance between MC-SC-RR and MC-SC-TC-RR gradually diminishes. For example, at Re = 100, the thermal resistance difference between MC-SC-RR and MC-SC-TC-RR is  $3.51 \text{ KW}^{-1}$ , while at Re = 400 and 800, this difference narrows to  $0.22 \text{ KW}^{-1}$  and  $0.16 \text{ KW}^{-1}$ , respectively. These findings show that the heat transfer enhancement resulting from the introduction of tertiary channels becomes more pronounced at higher Re.

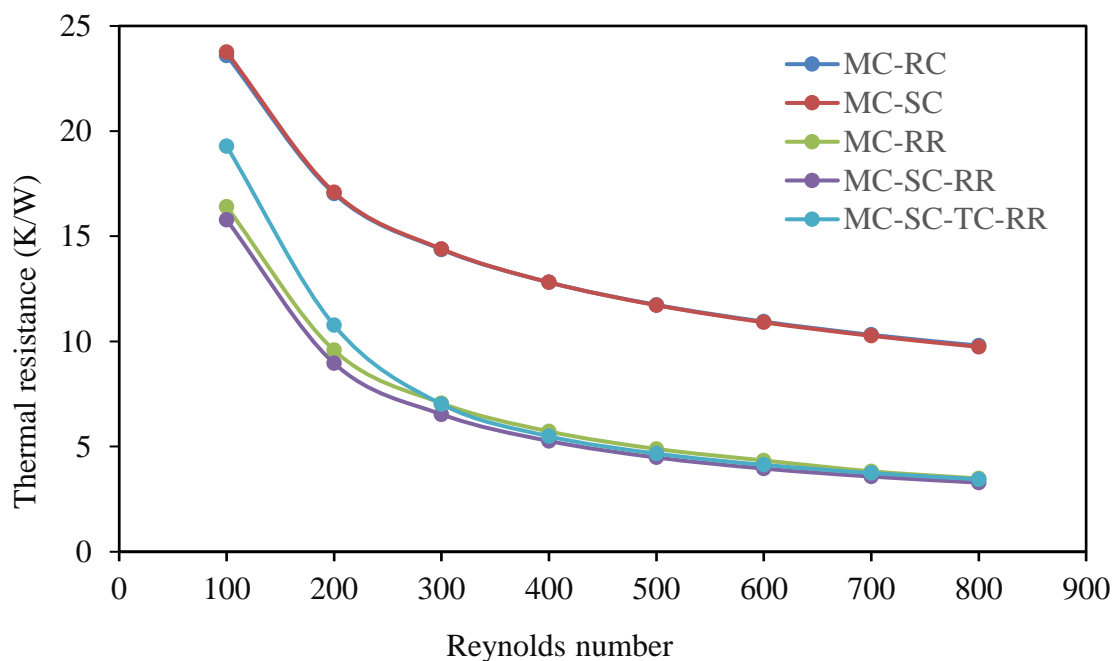


Fig. 15. Variation of total thermal resistance with Reynolds number for various microchannels

The performance of microchannels can also be compared under constant pumping power constraint, in addition to comparing them based on same Reynolds number. Figure 16 shows the relationship between total thermal resistance and pumping power for microchannel with different

geometry structures. In situations where pumping power is fixed, the microchannel that minimises the total thermal resistance is the preferred choice. It ensures optimised heat transfer efficiency and minimal energy consumption, which improves the overall performance of the microchannel. It can be observed that MC-RC and MC-SC have the highest total thermal resistance at different pumping power levels. Compared with these two cases, the utilisation of ribs in microchannel, as observed in MC-RR, can reduce the thermal resistance significantly. Constructing a microchannel with ribs and secondary channels, such as in MC-SC-RR, further reduces the thermal resistance. Across a variety of pumping power conditions, MC-SC-TC-RR consistently maintains a lower thermal resistance compared to other geometry structures.

The two methods outlined above are used to evaluate the performance of microchannels. However, the results of these two performance evaluation methods are vastly different. MC-SC-RR and MC-SC-TC-RR perform differently under different operating conditions. MC-SC-RR and MC-SC-TC-RR have the lowest thermal resistance at the same Reynolds number and at the constant pumping power, respectively. A pivotal issue that demands exploration is: which performance evaluation criteria is most relevant for assessing the overall performance of the microchannels? Optimal design of microchannel requires a compromise between maximising heat transfer performance and minimising pressure drop. The performance evaluation using Reynolds number is invaluable for investigating microchannel behaviour across various flow rates. It primarily focuses on understanding how flow rates impact heat transfer efficiency. However, this method does not directly account for hydraulic efficiency. On the contrary, the performance evaluation using pumping power offers a holistic approach. By considering both thermal and hydraulic efficiency, this method provides a comprehensive understanding of the overall performance of microchannels. The performance evaluation based on pumping power is more accurate, and it validates that the new design is the best performing microchannel.

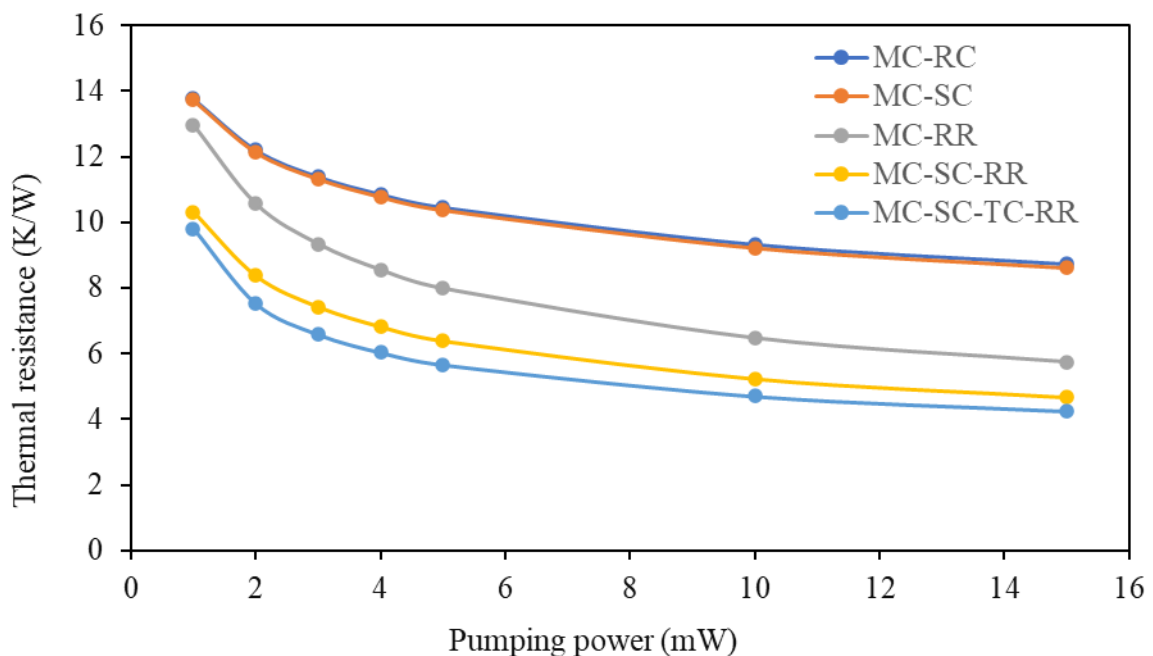


Fig. 16. Variation of total thermal resistance with pumping power for various microchannels

## 4. Conclusion

In this study, a novel microchannel integrating secondary channels, tertiary channels, and rectangular ribs is proposed. The cooling performance of this new design is compared with that of a conventional rectangular microchannel and enhanced microchannels using a three-dimensional solid fluid conjugate model. The present study leads to the following conclusions:

- i. The combination of microchannel features, such as secondary channels, tertiary channels, and rectangular ribs, has significantly enhanced the uniformity of flow velocity, particularly in the central portion of the channel.
- ii. The MC-SC-TC-RR design offers the largest convective heat transfer surface area compared to other designs, providing additional surface area for efficient heat exchange.
- iii. Adding tertiary channels and changing the rib orientation in MC-SC-RR significantly reduces the pressure drop caused by the flow blocking effect of ribs.
- iv. Changing the rib orientation enables the fluid to be redistributed into secondary channels and tertiary channels, which has positive impact on the heat transfer performance.
- v. MC-SC-TC-RR has the lowest total thermal resistance at various pumping power constraint, which indicates that it achieves a higher heat transfer rate than other microchannel designs at the same pumping power.

## References

- [1] Kandlikar, Satish G., and Akhilesh V. Bapat. "Evaluation of jet impingement, spray and microchannel chip cooling options for high heat flux removal." *Heat Transfer Engineering* 28, no. 11 (2007): 911-923. <https://doi.org/10.1080/01457630701421703>
- [2] Moore, Gordon E. "Cramming more components onto integrated circuits, Reprinted from Electronics, volume 38, number 8, April 19, 1965, pp. 114 ff." *IEEE solid-state circuits society newsletter* 11, no. 3 (2006): 33-35. <https://doi.org/10.1109/N-SSC.2006.4785860>
- [3] Franklin, Aaron D. "Nanomaterials in transistors: From high-performance to thin-film applications." *Science* 349, no. 6249 (2015): aab2750. <https://doi.org/10.1126/science.aab2750>
- [4] Nemati, H., M. A. Moghimi, and J. P. Meyer. "Shape optimisation of wavy mini-channel heat sink." *International Communications in Heat and Mass Transfer* 122 (2021): 105172. <https://doi.org/10.1016/j.icheatmasstransfer.2021.105172>
- [5] Khalifa, Mustafa Awaad, and Hayder Mohammad Jaffal. "Effects of channel configuration on hydrothermal performance of the cylindrical mini-channel heat sinks." *Applied Thermal Engineering* 148 (2019): 1107-1130. <https://doi.org/10.1016/j.applthermaleng.2018.11.101>
- [6] Jang, Seok Pil, Sung Jin Kim, and Kyung Wook Paik. "Experimental investigation of thermal characteristics for a microchannel heat sink subject to an impinging jet, using a micro-thermal sensor array." *Sensors and Actuators A: Physical* 105, no. 2 (2003): 211-224. [https://doi.org/10.1016/S0924-4247\(03\)00103-1](https://doi.org/10.1016/S0924-4247(03)00103-1)
- [7] Samadi, H., M. J. Hosseini, A. A. Ranjbar, and Y. Pahlavani. "Thermohydraulic performance of new minichannel heat sink with grooved barriers." *International Communications in Heat and Mass Transfer* 144 (2023): 106753. <https://doi.org/10.1016/j.icheatmasstransfer.2023.106753>
- [8] Ge, Ya, Shicheng Wang, Zhichun Liu, and Wei Liu. "Optimal shape design of a minichannel heat sink applying multi-objective optimization algorithm and three-dimensional numerical method." *Applied Thermal Engineering* 148 (2019): 120-128. <https://doi.org/10.1016/j.applthermaleng.2018.11.038>
- [9] Tuckerman, David B., and Roger Fabian W. Pease. "High-performance heat sinking for VLSI." *IEEE Electron device letters* 2, no. 5 (1981): 126-129. <https://doi.org/10.1109/EDL.1981.25367>
- [10] Lee, Y. J., P. S. Lee, and S. K. Chou. "Numerical study of fluid flow and heat transfer in the enhanced microchannel with oblique fins." *Journal of heat transfer* 135, no. 4 (2013): 041901. <https://doi.org/10.1115/1.4023029>
- [11] Japar, Wan Mohd Arif Aziz, Nor Azwadi Che Sidik, and Shabudin Mat. "A comprehensive study on heat transfer enhancement in microchannel heat sink with secondary channel." *International Communications in Heat and Mass Transfer* 99 (2018): 62-81. <https://doi.org/10.1016/j.icheatmasstransfer.2018.10.005>

- [12] Bahiraei, Mehdi, and Saeed Heshmatian. "Thermal performance and second law characteristics of two new microchannel heat sinks operated with hybrid nanofluid containing graphene–silver nanoparticles." *Energy conversion and management* 168 (2018): 357-370. <https://doi.org/10.1016/j.enconman.2018.05.020>
- [13] Qi, Zhina, Yuting Zheng, Junjun Wei, Xingang Yu, Xin Jia, Jinlong Liu, Liangxian Chen, Jianyin Miao, and Chengming Li. "Surface treatment of an applied novel all-diamond microchannel heat sink for heat transfer performance enhancement." *Applied Thermal Engineering* 177 (2020): 115489. <https://doi.org/10.1016/j.applthermaleng.2020.115489>
- [14] Loon, Yew Wai, and Nor Azwadi Che Sidik. "A comprehensive review of recent progress of nanofluid in engineering application: Microchannel heat sink (MCHS)." *Journal of Advanced Research in Applied Sciences and Engineering Technology* 28, no. 2 (2022): 1-25. <https://doi.org/10.37934/araset.28.2.125>
- [15] Japar, Wan Mohd Arif Aziz, Nor Azwadi Che Sidik, Siti Rahmah Aid, Yutaka Asako, and Tan Lit Ken. "A comprehensive review on numerical and experimental study of nanofluid performance in microchannel heatsink (MCHS)." *Journal of Advanced Research in Fluid Mechanics and Thermal Sciences* 45, no. 1 (2018): 165-176.
- [16] Perret, C., Ch Schaeffer, and J. Boussey. "Microchannel integrated heat sinks in silicon technology." In *Conference Record of 1998 IEEE Industry Applications Conference. Thirty-Third IAS Annual Meeting (Cat. No. 98CH36242)*, vol. 2, pp. 1051-1055. IEEE, 1998.
- [17] Wang, Hongtao, Zhihua Chen, and Jianguo Gao. "Influence of geometric parameters on flow and heat transfer performance of micro-channel heat sinks." *Applied Thermal Engineering* 107 (2016): 870-879. <https://doi.org/10.1016/j.applthermaleng.2016.07.039>
- [18] Lee, Yong-Jiun, Poh-Seng Lee, and Siaw-Kiang Chou. "Enhanced microchannel heat sinks using oblique fins." In *International Electronic Packaging Technical Conference and Exhibition*, vol. 43604, pp. 253-260. 2009. <https://doi.org/10.1115/InterPACK2009-89059>
- [19] Kuppusamy, Navin Raja, R. Saidur, N. N. N. Ghazali, and H. A. Mohammed. "Numerical study of thermal enhancement in micro channel heat sink with secondary flow." *International journal of heat and mass transfer* 78 (2014): 216-223. <https://doi.org/10.1016/j.ijheatmasstransfer.2014.06.072>
- [20] Ghani, Ihsan Ali, Nor Azwadi Che Sidik, Rizal Mamat, G. Najafi, Tan Lit Ken, Yutaka Asako, and Wan Mohd Arif Aziz Japar. "Heat transfer enhancement in microchannel heat sink using hybrid technique of ribs and secondary channels." *International Journal of Heat and Mass Transfer* 114 (2017): 640-655. <https://doi.org/10.1016/j.ijheatmasstransfer.2017.06.103>
- [21] Réti, Ferenc. "Liquid Cooling of Electronic Devices by Single-phase Convection (Wiley—Interscience Publication, 1999, New York—Chichester—Weinheim—Brisbane—Singapore—Toronto) Frank P. Incropera." *Journal of Thermal Analysis and Calorimetry* 58, no. 3 (1999): 749-749. <https://doi.org/10.1023/A:1010174209771>
- [22] Phillips, Richard J. "Microchannel heat sinks." *Advances in Thermal Modeling of Electronic Components* (1990).
- [23] Steinke, Mark E., and Satish G. Kandlikar. "Single-phase heat transfer enhancement techniques in microchannel and minichannel flows." In *International Conference on Nanochannels, Microchannels, and Minichannels*, vol. 41642, pp. 141-148. 2004. <https://doi.org/10.1115/ICMM2004-2328>
- [24] Lee, Y. J., P. S. Lee, and S. K. Chou. "Enhanced thermal transport in microchannel using oblique fins." (2012): 101901. <https://doi.org/10.1115/1.4006843>
- [25] Dewan, Anupam, and Pankaj Srivastava. "A review of heat transfer enhancement through flow disruption in a microchannel." *Journal of Thermal Science* 24 (2015): 203-214. <https://doi.org/10.1007/s11630-015-0775-1>